2016 American Control Conference (ACC)
Boston Marriott Copley Place
July 6-8, 2016. Boston, MA, USA

Using Inertial and Visual Sensing from a Mounted Smartphone to Stabilize a Ball and Beam Test-bed

Anthony Brill[1], Jared A. Frank[1], and Vikram Kapila[1]

***Abstract*— Mobile technology is developing and impacting society at an accelerating pace. Since their release in 2007, over one billion smartphones have reshaped the daily lives of their users and their embedded technologies have become increasingly more powerful and miniaturized with each new model. Yet, the majority of the most popular uses of these devices do not take full advantage of their sensing, storage, computation, and communication (SSCC) capabilities. In this paper, we consider an experimental setup in which a smartphone is mounted to a ball and beam system using a 3D-printed mounting structure attached at each end of the beam. To perform feedback control of the ball and beam system, the smartphone's inertial and camera sensors are used to measure the angular orientation and velocity of the beam and translational position of the ball on the beam. To account for the nonlinear effects added to the system by the presence of the smartphone and its mounting structure, a feedback linearizing controller is used to stabilize the system. Simulation and experimental results are presented to show that smartphones and their various sensors can be integrated in the wireless sensing and control of physical systems as part of an emerging class of smartphone-mounted test-beds for research and education.**

I. Introduction

Recent years have experienced a significant increase in the accessibility of smart mobile devices, creating the need to explore potential uses of the embedded sensors housed in these devices. Smartphones in particular have now been so heavily integrated into daily life that individuals have their personal devices on them at all times of the day. Currently, the on-board sensors of smartphones are not being used to their full potential. Today's smartphones have the ability to offer educators, researchers, and students with a complete SSCC platform. As of now, smartphones are being used for only basic sensing applications such as tilt-based video games, detection of metal objects from magnetometer measurements, navigation using GPS information, demonstration of angular momentum conservation using the gyroscope [14], etc. The SSCC capabilites of these devices remain to be fully explored and have the potential to be integrated into the closed-loop feedback control of physical systems.

One of the most powerful sensors on smart mobile devices is the camera. Image-based visual servoing (IBVS) is commonly used for feedback control applications in which the deviations of features in an image are used to calculate control actions, offering contactless measurements to control a system such as ball and beam [4], [7], [13]. IBVS approaches have been investigated in the eye-to-hand configuration [3], [8], in which a camera fixed in the environment points towards the experiment, either from above the test-bed to measure ball position [7] or along the rotational axis of the beam to measure angular motion [13]. Tablet computers have also been used to demonstrate the ability to stabilize a ball and beam system by measuring both beam angle and ball position in an eye-to-hand configuration [5]. However, the compact form factor of smartphones provides the opportunity to explore the eye-in-hand configuration, which involves attaching the camera to the system being controlled, e.g., as in feedback control of surgical instruments [10].

Fig. 1: A smartphone-mounted ball and beam system.

Inertial measurement units (IMU) have become a standard sensor on-board smartphones and typically consist of a 3-axis gyroscope, accelerometer, and magnetometer. The IMU provides valuable measurements for feedback control of a translating and/or rotating mechanical system. The IMU is often introduced into gaming applications on smart devices to increase interactivity. Moreover, its application in feedback control has also been explored in the wireless control of a DC motor to regulate the position of the motor arm [6].

The implementation of mounted smartphones as platforms in feedback control of lab experiments can provide novel inquiry-based educational and research experiences. For many applications, the multimodal sensing capabilities of these devices allow the smartphone to act as a complete sensing platform, which can significantly reduce the cost and complexity of the system. In this paper, we investigate a eye-to-hand implementation of IBVS to stabilize a ball and beam test-bed using a mounted smartphone to measure the position of the ball through image data and the rotational states of the system through inertial measurements. In Section II, an overview of the system and user interface are presented. Section III describes the techniques used by the mobile application to obtain inertial and vision-based measurements

This work is supported in part by the National Science Foundation awards RET Site EEC-1132482, GK-12 Fellows DGE: 0741714, and DRK-12 DRL: 1417769, and NY Space Grant Consortium grant 76156-10488.

[1]Mechatronics and Controls Lab, Mechanical and Aerospace Engineering, NYU Tandon School of Engineering, Brooklyn, NY 11201 [brill.anthony, jared.alan, vkapila]@nyu.edu

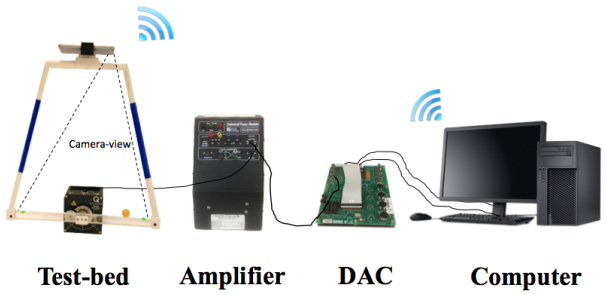

Fig. 2: Schematic representation of the ball and beam control system with a mounted smartphone.

of the beam and ball state variables, respectively. Section IV discusses the dynamic model of the ball and beam test-bed and the feedback linearization approach used to compensate for nonlinearities in the model while stabilizing the closed-loop system. Section V presents the results of simulations and experiments conducted with the smartphone-mounted system. Section VI offers some concluding remarks.

II. System Description

The system used in this study is a ball and beam test-bed with a smartphone mounted to the beam using a 3D-printed plastic structure. The motorized beam is driven using a power amplifier which receives control signals from a personal computer (PC) via a data acquisition and control (DAC) board. The mounted smartphone is responsible for all sensing on the system. The mobile application running on the smartphone uses inertial measurements and visual observations of the ball to measure three out of the four states of the system. Measurements are transmitted over a Wi-Fi network to the PC, which performs partial state estimation and computes and relays control signals to the test-bed using the MATLAB/Simulink environment. The components of the proposed system are shown in Figure 2.

The smartphone used in this study is an Apple iPhone 6 Plus, which has a 5.5 inch (140 mm), 1080×1920 pixel multi-touch display, 1.4 GHz dual-core processor, an InvenSense MP67B 6-Axis MEMS IMU, and a 8-megapixel rear-facing camera. Both an InvenSense IMU and Bosch BMA280 three-axis accelerometer are integrated in the iPhone 6 Plus. The IMU is configurable to operate in either a six-axis inertial sensor mode, three-axis gyroscope mode, or a three-axis accelerometer mode, with rated current consumption of 3.4 mA, 3.2 mA, and 450 uA, respectively. A major advantage of the IMU is full six-axis integration of data by a digital motion processor (DMP) located on the chip. The DMP provides 16-bit readings that have benefited gaming and other applications requiring sophisticated inertial sensing. At the expense of higher power consumption, the IMU provides significantly higher sensitivity. While both the BMA280 and the accelerometer of the IMU can sense accelerations of up to 16g, the BMA280 is utilized in applications where full six-axis readings are not needed and lower sensitivity is allowable, such as adjusting screen orientation and pedometry, in exchange for reduced power consumption. Only the IMU is implemented for the purposes of this study.

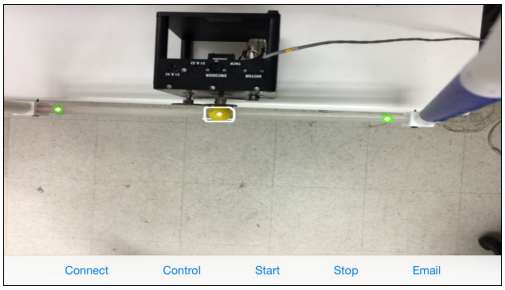

Fig. 3: Screenshot of the user interface.

Since the smartphone is rigidly mounted to the test-bed, the motion of the phone obtained with the IMU can be used to describe the motion of the beam about its rotational axis. The rear-facing camera of the iPhone 6 Plus supports frame rates of only up to 30 frames per second (fps) at image resolutions below 1280×720 pixels. An image processing routine (see subsection III-A) running in the background of the mobile application is used to extract measurements of the ball position.

In addition to offering its on-board sensing capabilities to control the ball and beam test-bed, the smartphone also allows for the design and implementation of an interactive user interface that is mounted to the experiment. The mobile application developed for this experiment contains buttons that allow users to wirelessly connect to the PC, start and stop the experiment, and email experimental data for further analysis. The touch screen display on the smartphone allows users to select the ball's reference position on the beam, and displays useful visual feedback to the user regarding the data collected by the application and the status of the image processing algorithm used to compute the ball position. This allows users to easily calibrate and troubleshoot the system.

III. Vision-based and Inertial Measurements

Rigidly mounting the smartphone to the ball and beam system allows for both visual and inertial measurements of state variables. In this section, we describe the image processing techniques used to detect the ball position and the methodology used to determine beam angle and angular velocity using the inertial sensors.

A. Ball Position Measurement

To perform vision-based detection of the ball position, the ball is painted yellow and a green marker is attached at each end of the beam. Each of the three colored objects is detected using a color segmentation approach involving thresholding in the hue-saturation-value (HSV) space and morphological filtering operations to remove small amounts of noise [5]. Because the smartphone is mounted such that the user interface is accessible to the user, the back-facing camera is used to obtain vision-based measurements of the ball position at a frequency of 30 Hz. A 3D-printed trapezoidal mounting structure is constructed to rigidly mount the smartphone at a height above the beam that allows the ball to be observed as it travels along the entire length of the beam. Knowledge of the smartphone's rigid attachment to the structure is

exploited to create narrow search spaces for each of the colored objects. Since the locations of the markers at the ends of the beam do not move relative to the camera, square search regions are hard-coded into the application to search for the green markers. The search space for the ball is defined as a thin strip around the location of the beam in the video frames. This technique allows for the image processing on the smartphone to be made significantly more efficient, thus allowing the satisfaction of real-time constraints that preserve the stability of the closed-loop system [1], [5]. Calculating the position of the ball along the beam involves finding the distance in pixels between the image coordinates of the detected ball, $p_{\mathrm{b}} = (x_{\mathrm{b}}, y_{\mathrm{b}})$, and the marker on the left end of the beam, $p_{\ell} = (x_{\ell}, y_{\ell})$, as well as the distance between the left marker and the marker at the right end of the beam, $p_{\mathrm{r}} = (x_{\mathrm{r}}, y_{\mathrm{r}})$. Then, the normalized ball position x_{norm} is found as follows

$$x_{\mathrm{norm}} = \frac{p_{\mathrm{b}} - p_{\ell}}{p_{\mathrm{r}} - p_{\ell}}. \tag{1}$$

This result can be viewed as the percentage that the ball has traveled along the length of the beam from left to right. Knowing the distance l in real-world units between the markers, measurements for the ball position x are obtained with respect to the point halfway between the markers

$$x = (x_{\mathrm{norm}} - 0.5) \times l. \tag{2}$$

B. Beam Angle and Angular Velocity Measurements

Since the trapezoidal structure rigidly mounts the smartphone to the beam, the beam, structure, and phone can be viewed as a rigid body. Thus, the IMU of the smartphone is used to capture the rotational motion of the structure. Filtered data from the gyroscope about the rotational axis of the phone is used as the measurement of the structure's angular velocity. To measure angular orientation, readings of device attitude are generated after raw accelerometer and gyroscope data are processed by the device's sensor fusion algorithms. Device attitude is expressed as the rotation between the device's current reference frame and a reference frame that is formed using the direction of gravity obtained from the accelerometer. The angle and angular velocity measurements are periodically requested by the mobile application at a frequency of 90 Hz. To synchronize inertial measurements with vision-based measurements, so that all measurements are transmitted wirelessly in a single TCP/IP packet, the update interval of the inertial measurements is chosen as an integer multiple of the vision-based measurements.

IV. Modeling and Control

To control the ball and beam test-bed and allow the ball to track a step reference command using visual and inertial feedback from the smartphone, a nonlinear, dynamic model of the plant is obtained in this section. This nonlinear model is used in the design of a feedback linearizing controller, which is implemented on the PC in the Matlab/Simulink environment, to stabilize the system.

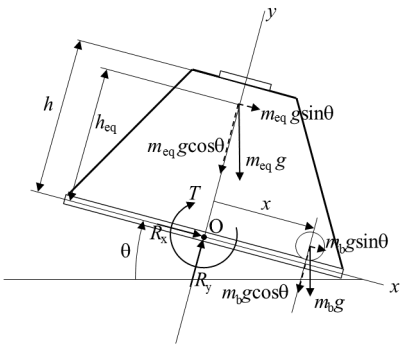

Fig. 4: Model of the smartphone-mounted ball and beam.

A. Plant Model

A diagram of the ball and beam system with the mounting structure and smartphone is shown in Figure 4. The system is modeled in three separate parts: (1) a DC motor whose electromechanical behavior is captured; (2) the beam, plastic 3D-printed trapezoidal mounting structure, and smartphone mounted at the top of the structure, whose rotational dynamics introduces a nonlinearity; and (3) a yellow plastic ball whose translational motion along a v-shaped groove on the top surface of the beam is described. The control objective is to stabilize the ball and beam system such that the ball can track a step reference command, using measurements of the ball position, beam angle, and beam angular velocity. The ball is at a position x in meters and the beam is oriented at an angle θ in radians. A small amount of friction is present between the motor shaft and beam.

When a voltage V is applied to the DC motor of the test-bed, it produces a torque T_{m} that is directly proportional to the motor current, which is determined using Kirchoff's voltage law. A gearbox with gear ratio K_{g} processes the motor torque T_{m} to produce the torque T applied to the beam

$$T = K_{\mathrm{g}} T_{\mathrm{m}} = K_{\mathrm{g}} K_{\mathrm{T}} i_{\mathrm{a}} = -\frac{K_{\mathrm{b}} K_{\mathrm{g}}^2 K_{\mathrm{T}}}{R_{\mathrm{a}}} \dot{\theta} + \frac{K_{\mathrm{g}} K_{\mathrm{T}}}{R_{\mathrm{a}}} V, \tag{3}$$

where i_{a} is the electric current through the motor circuit, R_{a} is the resistance in the motor circuit, K_{T} is the motor-torque constant, K_{b} is the back-emf constant, and $\dot{\theta}$ is the rotational velocity of the output shaft of the gearbox. Note that even as an inductor in the motor's armature circuit introduces dynamic characteristics, the test-bed motor's small armature inductance (0.18 mH) [1] yields a time constant for the electrical system dynamics that is two orders of magnitude smaller than the time constant of the mechanical system dynamics driven by the motor, thus the electrical system dynamics are safely neglected to yield (3).

The torque T exerted by the gearbox onto the combined beam, trapezoidal mounting structure, and smartphone drives the rotational dynamics of the mechanical system whose equations of motion can be derived using a Newtonian approach. To begin, note that with m_{sm} denoting the mass of the smartphone with center of mass located at $(0, h)$ and m_{st} denoting the mass of the structure with center of mass located at $(0, \frac{2}{3}h)$, the equivalent mass of the smartphone and trapezoidal mounting structure can be denoted by $m_{\mathrm{eq}} \triangleq m_{\mathrm{sm}} + m_{\mathrm{st}}$

with its center of mass located at $h_{\rm eq} \triangleq \frac{hm_{\rm sm}+0.67hm_{\rm st}}{m_{\rm eq}}$. Next, taking the sum of the moments about point O yields

$$I\ddot{\theta} = m_{\rm eq}gh_{\rm eq}\sin\theta + m_{\rm b}gr_{\rm b}\sin\theta + m_{\rm b}gx\cos\theta - b_{\rm t}\dot{\theta} + T, \quad (4)$$

where g is the acceleration under gravity, $r_{\rm b}$ is the radius of the ball, $b_{\rm t}$ is a viscous damping term, and I is the sum of the moments of inertia of the beam, trapezoidal mounting structure, and smartphone about the rotational axis. Neglecting the mass of the ball relative to the mass of the beam, phone, and structure and solving for the angular acceleration of the beam gives

$$\ddot{\theta} = \frac{m_{\rm eq}gh_{\rm eq}}{I}\sin\theta - \frac{b_{\rm t}}{I}\dot{\theta} + \frac{1}{I}T. \quad (5)$$

An Euler-Lagrange approach is used to derive the dynamics of the ball rolling on the beam [2], [5], yielding

$$\left(\frac{I_{\rm b}}{r_{\rm b}^2} + m_{\rm b}\right)\ddot{x} + m_{\rm b}x\dot{\theta}^2 - m_{\rm b}g\sin\theta = 0, \quad (6)$$

where $I_{\rm b} = \frac{2}{5}m_{\rm b}r_{\rm b}^2$ is the mass moment of inertia of the spherical ball about a centroidal axis. Assuming small and slow changes in beam angle (so that $\dot{\theta}^2 \approx 0$), we have the following dynamics of the ball motion

$$\ddot{x} = \frac{m_{\rm b}g}{I_{\rm b}/r_{\rm b}^2 + m_{\rm b}}\sin\theta. \quad (7)$$

Combining the results of the electrical subsystem (3), beam and structure dynamics (5), and ball dynamics (7) yields the complete dynamics of the system. After choosing a state vector $\mathbf{x} \triangleq [x \quad \dot{x} \quad \theta \quad \dot{\theta}]^{\rm T}$ and output $y = x$ (see the step reference tracking problem discussed in Section IV-B), the equations of motion are expressed as follows

$$\begin{aligned} \dot{x}_1 &= x_2, \\ \dot{x}_2 &= \gamma\sin x_3, \\ \dot{x}_3 &= x_4, \\ \dot{x}_4 &= \mu\sin x_3 - \sigma x_4 + \delta u, \\ y &= x_1, \end{aligned} \quad (8)$$

where x_i, $i = 1,\ldots,4$, are components of $\mathbf{x}$, $\gamma \triangleq \frac{m_{\rm b}g}{I_{\rm b}/r_{\rm b}^2+m_{\rm b}}$, $\mu \triangleq \frac{m_{\rm eq}gh_{\rm eq}}{I}$, $\sigma \triangleq \left(\frac{b_{\rm t}}{I} + \frac{K_{\rm b}K_{\rm g}^2K_{\rm T}}{IR_{\rm a}}\right)$, and $\delta \triangleq \frac{K_{\rm g}K_{\rm T}}{IR_{\rm a}}$. Although the dynamics of (8) are nonlinear, this system is both input-state and input-output linearizable. Specifically, consider the following change of variables

$$\xi \triangleq T(x) = \begin{bmatrix} x_1 & x_2 & \gamma\sin x_3 & \gamma x_4\cos x_3 \end{bmatrix}^{\rm T}, \quad (9)$$

that transforms (8) into the normal form [9]

$$\dot{\xi} = A_{\rm c}\xi + B_{\rm c}\beta^{-1}[u - \alpha(x)], \quad y = C_{\rm c}\xi, \quad (10)$$

where

$$A_{\rm c} \triangleq \begin{bmatrix} 0 & 1 & 0 & 0 \\ 0 & 0 & 1 & 0 \\ 0 & 0 & 0 & 1 \\ 0 & 0 & 0 & 0 \end{bmatrix}, \; B_{\rm c} \triangleq \begin{bmatrix} 0 \\ 0 \\ 0 \\ 1 \end{bmatrix}, \; C_{\rm c} \triangleq \begin{bmatrix} 1 \\ 0 \\ 0 \\ 0 \end{bmatrix}^{\rm T},$$

$$\alpha(x) \triangleq -\frac{1}{\delta\gamma\cos x_3}\left[-\gamma x_4^2\sin x_3 + \gamma\cos x_3\,(\mu\sin x_3 - \sigma x_4)\right],$$

$$\beta(x) \triangleq \frac{1}{\delta\gamma\cos x_3}, \quad x_3 \neq \pm\frac{\pi}{2}.$$

The numerical values for the physical parameters of laboratory ball and beam system are provided in Table I below.

TABLE I: Numerical values for physical parameters of the ball and beam test-bed.

Physical quantity	Symbol	Numerical value	Units
Ball mass	$m_{\rm b}$	0.007	kg
Smartphone mass	$m_{\rm sm}$	0.172	kg
Structure mass	$m_{\rm st}$	0.217	kg
Ball radius	$r_{\rm b}$	0.013	m
Smartphone height	h	0.5	m
Gravitational constant	g	9.8	m/s^2
Moment of Inertia	I	0.06711	kg·m^2
Back-emf constant	$K_{\rm b}$	0.00768	Volt·s/rad
Motor torque constant	$K_{\rm T}$	0.00768	N·m/Amp
Friction coefficient	$b_{\rm t}$	0.05	N·m·s
DC-motor resistance	$R_{\rm a}$	2.6	Ω
Gear ratio	$K_{\rm g}$	14	

B. Step Command Tracking with Integral Control

Our objective is to control the system so that the ball position $y(t) = x(t)$ tracks a step command r issued by the user by tapping on the touchscreen of the smartphone. Therefore, an integrator state $\dot{\rho} = e$, where $e \triangleq y - r = x_1 - r$, is augmented to (10) as in [9]

$$\dot{\xi}_{\rm a} = A\xi_{\rm a} + B\beta^{-1}[u - \alpha(x)], \quad (11)$$

where

$$A \triangleq \begin{bmatrix} A_{\rm c} & 0 \\ C_{\rm c} & 0 \end{bmatrix}, \quad B \triangleq \begin{bmatrix} B_{\rm c} \\ 0 \end{bmatrix},$$

$$Y_{\rm r} \triangleq \begin{bmatrix} r & 0 & 0 & 0 \end{bmatrix}^{\rm T}, \quad \xi_{\rm a} \triangleq \begin{bmatrix} E \\ \rho \end{bmatrix}, \quad E \triangleq \xi - Y_{\rm r}.$$

C. Discretization and Controller Design

By applying the state feedback linearizing control

$$u = \alpha(x) + \beta v, \quad (12)$$

the $\xi_{\rm a}$ system of (11) is linearized to the following form

$$\dot{\xi}_{\rm a} = A\xi_{\rm a} + Bv. \quad (13)$$

Since measurement data is transmitted by the smartphone at a finite rate, the state-space model of the feedback linearized dynamics of (13) is discretized at each sampling instant kT, $k = 0,1,2,\ldots$, with $T = 1/90$ seconds, to yield the following sampled-data model

$$\xi_{\rm a}[(k+1)T] = \Phi\xi_{\rm a}[kT] + \Theta v[kT], \quad (14)$$

where $\Phi \triangleq e^{AT}$ is the state transition matrix of the resulting model and $\Theta \triangleq \int_0^T e^{A(T-\tau)}B{\rm d}\tau$. Before designing a linear quadratic regulator (LQR) for the sampled-data model with sampling time T, the controllability of system (14) is verified by confirming that the controllability matrix M_c is of full rank

$$M_c = \begin{bmatrix} \Theta & \Phi\Theta & \Phi^2\Theta & \Phi^3\Theta \end{bmatrix}.$$

Next, the LQR approach is applied to (Φ,Θ) to design a full-state feedback controller $v[kT] = K_{\rm c}\xi_{\rm a}[kT]$, where $K_{\rm c}$ is the control gain, that minimizes the quadratic cost function $J(u)$

$$J(u) = \sum_{k=1}^{\infty}(\xi_{\rm a}^{\rm T}[kT]R_1\xi_{\rm a}[kT] + v^{\rm T}[kT]R_2v[kT]), \quad (15)$$

where R_1 is nonnegative-definite and R_2 is a positive-definite. The control gain K_c is obtained from $K_c = (\Theta^T P \Theta + R_2)^{-1}(\Theta^T P \Phi)$, where P is the solution to the discrete-time algebraic Riccati equation [16]

$$P = \Phi^T P \Phi + R_1 - (\Theta^T P \Phi)^T (\Theta^T P \Theta + R_2)^{-1} (\Theta^T P \Phi). \quad (16)$$

The feedback control K_c is designed such that errors in ball position and ball velocity are penalized more than deviations in beam angle and velocity with the weighting matrix $Q = [1800 \quad 15 \quad 0 \quad 0 \quad 20]^T$. The control penalty $R_2 = 0.15$ is chosen from simulation tests to limit the range of control voltage to the motor to within an allowable range and the control signal is saturated to $\pm$ 15 Volts.

D. State Estimation

The proposed smartphone-mounted sensing approach outlined in this paper provides measurements for three of the four original states of the system: IMU-based measurements (at 90 Hz) of angular position and angular velocity of the beam, and vision-based measurements (at 30 Hz) of ball position. State estimation is necessitated because (i) the velocity of ball is not measured directly and (ii) ball position measurement from the smartphone camera is corrupted by noise. To handle measurement updates occurring at two rates, common practices are to either down-sample the faster sensors to the rate of the slower ones and design a single-rate estimator updating at the slower rate or to update the system states corresponding to the slower sensors via an estimator updating at the faster rate during inter-sample periods [15]. In this paper, we design an estimator for the partial state vector (i.e., $\mathbf{x}_p \triangleq [x_1 \quad x_2]^T$) to obtain estimates (at 90 Hz) for ball position and velocity using the dynamics of the ball and the measurement of ball position, y (available at 30 Hz). Letting $\hat{u} \triangleq \sin x_3$, the following state-space model characterizes the estimator dynamics for ball position and ball velocity estimates, $\hat{\mathbf{x}}_p \triangleq [x_{1e} \quad x_{2e}]^T$

$$\begin{aligned}\hat{\mathbf{x}}_p[(k+1)T] = &\exp\left(\begin{bmatrix} 0 & 1 \\ 0 & 0 \end{bmatrix} T\right) \hat{\mathbf{x}}_p[kT] \\ &+ \int_0^T \exp\left(\begin{bmatrix} 0 & 1 \\ 0 & 0 \end{bmatrix} (T-\tau)\right) \begin{bmatrix} 0 \\ \gamma \end{bmatrix} d\tau \, \hat{u}[kT] \\ &+ L\left(y[kT] - \begin{bmatrix} 1 & 0 \end{bmatrix} \hat{\mathbf{x}}_p[kT]\right), \end{aligned} \quad (17)$$

where L is the observer gain designed to place the eigenvalues of the estimation error dynamics at $(-0.5, -0.5)$ [11]. Next, (17) can be used to produce state estimates $\hat{\mathbf{x}}_p$ in two ways. First, we can set $y[kT] = x_{1e}[kT]$ at inter-sample periods $(k+1)T$ and $(k+2)T$, $k = 0, 3, 6, \ldots$, that is equivalent to setting $L = 0$ at inter-sample periods [15]. Second, we can hold $y[kT]$ constant at inter-sample periods. In subsection V-B below, we examine both these methods with simulations and experiments and illustrate that with y sampled at 30 Hz both methods yield comparable results.

V. Simulation and Experimental Results

In this section, we describe simulation and experimental results which show that, in spite of the challenges posed by the mounted smartphone, the ball and beam test-bed yields acceptable performance in tracking step commands and in response to disturbances. See [12] for an illustrative video of the experiment.

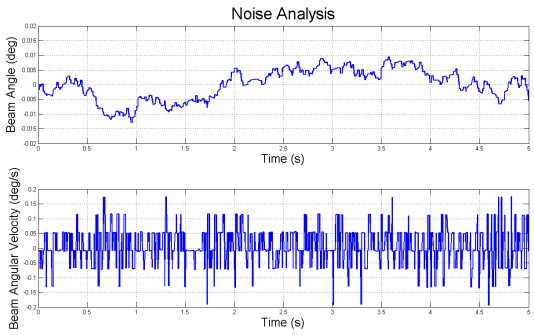

Fig. 5: Raw sensor data collected while the system is at rest.

A. Measurement Precision

To investigate the noise characteristics of the angle and angular velocity measurements provided by the smartphone, raw data is obtained from the smartphone while mounted to the ball and beam test-bed as it is resting in its zero configuration and not being controlled. The raw sensor data is shown in Figure 5. The data is collected over a course of 5 seconds at a sampling rate of 90 Hz. Because the orientation measurement of the smartphone is provided by the device's built-in sensor fusion estimation algorithms that use measurements from the IMU, a small amount of drift is seen in the orientation measurement. It can be seen in Figure 5 that the beam angle reported by the phone has a range of 0.022° and the beam angular velocity has a variance of 0.0041. Due to constraints on the sampling rate of the camera, vision-based measurements are restricted to 30 Hz, which in turn restricts the image processing routine to approximately 33 ms. At this sampling rate, the highest allowable image resolution is 640×480 before the computation time exceeds the allowable range. The average computation time for the image processing routine is found to be 30.24 ms with a standard deviation of 0.6541 ms. While computation time can be reduced by using a lower resolution image, the measurement precision of ball position will be jeopardized. At an image resolution of 640×480, the ball position can be measured with a resolution of 0.705 mm.

B. Step Command Tracking

Limitations and coupling between the resolution, precision, and update rate associated with the IMU and camera onboard the smartphone can have consequences on the stability and performance of the closed-loop system. Specifically, while lowering the image resolution to 352×288 degrades measurement precision, increasing the image resolution to 1280×720 yields larger computation delays, both of which rendered the system unstable in experiments. To investigate the system response to step reference commands, a simulation and an experiment are performed (see Figure 6). User applied taps on the touchscreen generate reference

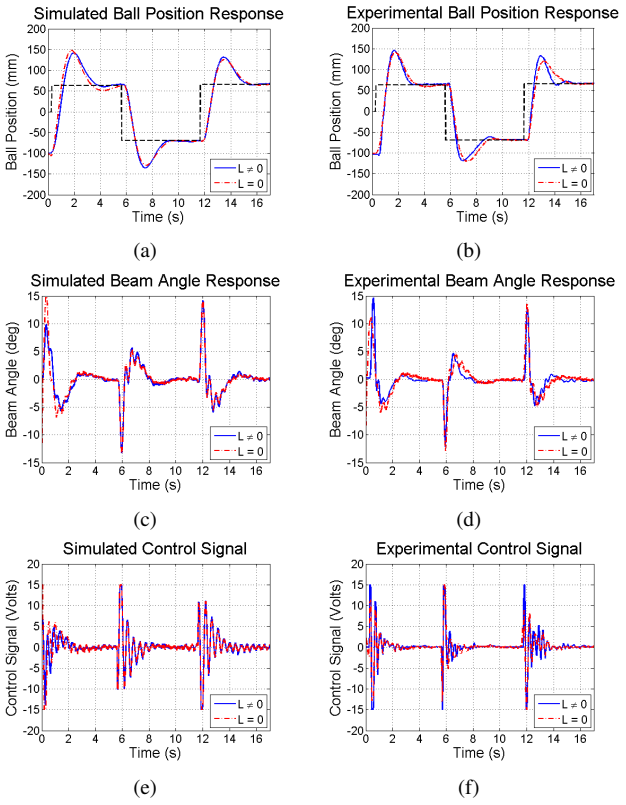

Fig. 6: System response for step reference simulation (a, c, e) and experiments (b, d, f) with two methods to estimate $\hat{\mathbf{x}}_p$ (IMU and camera sampling at 90 Hz and 30 Hz, respectively).

commands that are used for both simulations and experiments. The ball and beam system is simulated taking into account experimentally observed sensor noise, computation and communication delays, measurement resolution, sampling rates, and actuator saturation. The system is simulated by using two methods of subsection IV-D to estimate $\hat{\mathbf{x}}_p$ and the resulting closed-loop responses in Figure 6(a) are found to be comparable. Space constraints do not allow inclusion of additional simulation results that show the following: (i) the closed-loop system performance improves as delay, measurement resolution, and sampling period of the vision-based measurements are each lowered and (ii) the inertia of the structure and phone limit the achievable performance of the closed-loop system. Figures 6(a, c, e) present the simulated responses and Figures 6(b, d, f) present the experimental responses, illustrating that simulated and experimental responses are comparable. To evaluate the system's ability to recover from disturbances, the ball is pushed far from its stabilized reference position at the center of the beam. Figure 7 presents the disturbance response of the ball position and beam angle. It is observed that the system requires approximately 3.5 seconds for its response to adequately settle.

VI. Conclusion

This paper presented a mobile application that uses the inertial sensors and back-facing camera on-board a smartphone to obtain measurements for the feedback control of a ball and beam test-bed to which the smartphone is rigidly mounted. Future work will investigate the effectiveness and user experience associated with the use of the proposed system in inquiry-based learning with the personal devices of students and researchers in classrooms and laboratories.

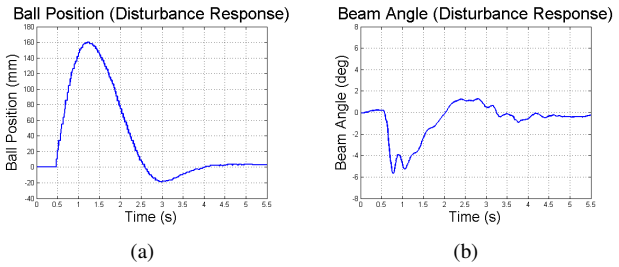

Fig. 7: Ball position (a) and beam angle (b) response to a disturbance.

References

[1] J. Apkarian, *A Comprehensive and Modular Laboratory for Control Systems Design and Implementation*. Quanser Consulting, 1995.

[2] C. Bolívar and G. Beauchamp, "Modelling the ball-and-beam system from Newtonian mechanics and from Lagrange methods," in *Proc. Latin American and Carribbean Conf. on Engineering and Technology*, 2014, p. 176.

[3] F. Chaumette and S. Hutchinson, "Visual servo control part II: Advanced approaches," *IEEE Robotics & Automation Magazine*, vol. 14, no. 1, pp. 109–118, 2007.

[4] E. P. Dadios *et al.*, "Vision guided ball-beam balancing system using fuzzy logic," in *IEEE Industrial Electronics Society.*, vol. 3, 2000, pp. 1973–1978.

[5] J. A. Frank, J. A. De Gracia Gomez, and V. Kapila, "Using tablets in the vision-based control of a ball and beam test-bed," in *Proc. Int. Conf. Informatics in Control, Automation, and Robotics*, Colmar, Alsace, France, 2015, pp. 92–102.

[6] J. A. Frank *et al.*, "Exploring the role of a smartphone as a motion sensing and control device in the wireless networked control of a motor test-bed," in *Proc. Int. Conf. Informatics in Control, Automation, and Robotics*, Colmar, Alsace, France, 2015, pp. 328 – 335.

[7] I. Hasanzade, S. Anvar, and N. Motlagh, "Design and implementation of visual servoing control for ball and beam system," in *Int. Symp. on Mechatronics and Its Applications.*, 2008, pp. 1–5.

[8] S. Hutchinson, G. Hager, and P. Corke, "A tutorial on visual servo control," *IEEE Trans. Robotics and Automation*, vol. 12, no. 5, pp. 651–669, 1996.

[9] H. K. Khalil, *Nonlinear Systems*. Prentice Hall, Upper Saddle River, NJ, 2001, vol. 3.

[10] A. Krupa *et al.*, "Autonomous 3-d positioning of surgical instruments in robotized laparoscopic surgery using visual servoing," *IEEE Trans. Robotics and Automation*, vol. 19, no. 5, pp. 842–853, 2003.

[11] R. H. Middleton and G. C. Goodwin, *Digital Control and Estimation: A Unified Approach*. Prentice Hall, Englewood Cliffs, NJ, 1990.

[12] NYU. (2016) Stabilizing a ball and beam test-bed with a mounted smartphone. [Online]. Available: http://engineering.nyu.edu/mechatronics/videos/ballbeamstabilize.html.

[13] I. Petrović, M. Brezak, and R. Cupec, "Machine vision based control of the ball and beam," in *Int. Workshop on Advanced Motion Control*, 2002, pp. 573–577.

[14] A. Shakur and T. Sinatra, "Angular momentum," *The Physics Teacher*, vol. 51, no. 9, pp. 564–565, 2013.

[15] Y. Wang *et al.*, "Multirate estimation and control of body slip angle for electric vehicles based on onboard vision system," *IEEE Trans. Industrial Electronics*, vol. 61, no. 2, pp. 1133–1143, 2014.

[16] K. Zhou, J. Doyle, and K. Glover, *Robust and Optimal Control*. Prentice Hall, Englewood Cliffs, NJ, 1996.